

Surface Properties of Nanocrystalline PbS Films Deposited at the Water–Oil Interface: A Study of Atmospheric Aging

David J. H. Cant,[†] Karen L. Syres,^{†,⊥} Patrick J. B. Lunt,[†] Hanna Radtke,[†] Jon Treacy,^{†,‡} P. John Thomas,^{†,#} Edward A. Lewis,[‡] Sarah J. Haigh,[‡] Paul O'Brien,[‡] Karina Schulte,[§] Federica Bondino,^{||} Elena Magnano,^{||} and Wendy R. Flavell*,[†]

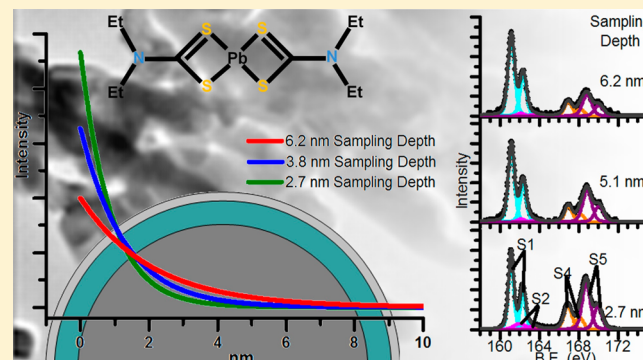
[†]School of Physics and Astronomy and the Photon Science Institute, and [‡]School of Materials, The University of Manchester, Manchester M13 9PL, United Kingdom

[§]MAX-lab, Lund Universitet, Ole Römers väg 1, SE-223 63 Lund, Sweden

^{||}IOM CNR, Laboratorio Nazionale TASC, Area Science Park - Basovizza, S.S. 14 Km. 163,5, I-34149 Basovizza, Trieste, Italy

Supporting Information

ABSTRACT: Nanocrystalline thin films of PbS are obtained in a straightforward reaction by precipitation at the interface between toluene (containing a Pb precursor) and water (containing Na₂S). Lead thiobiuret [Pb(SON(CNⁱPr₂)₂)] and lead diethyldithiocarbamate [Pb(S₂CNEt₂)₂] precursors are used. The films are characterized by X-ray diffraction and electron microscopy, revealing typical particle sizes of 10–40 nm and preferred (200) orientation. Synchrotron-excited depth-profiling X-ray photoelectron spectroscopy (XPS) is used to determine the depth-dependent chemical composition as a function of surface aging in air for periods of up to 9 months. The as-synthesized films show a 1:1 Pb/S composition. Initial degradation occurs to form lead hydroxide and small quantities of surface-adsorbed –SH species. A lead-deficient Pb_{1-x}S phase is produced as the aging proceeds. Oxidation of the sulfur occurs later to form sulfite and sulfate products that are highly localized at the surface layers of the nanocrystals. These species show logarithmic growth kinetics, demonstrating that the sulfite/sulfate layer acts to passivate the nanocrystals. Our results demonstrate that the initial reaction of the PbS nanocrystals (forming lead hydroxide) is incongruent. The results are discussed in the context of the use of PbS nanocrystals as light-harvesting elements in next-generation solar technology.



1. INTRODUCTION

Lead sulfide, PbS, is an important direct band gap semiconductor material, with a gap of 0.41 eV.¹ This may be increased by quantum confinement such that PbS nanocrystals (NCs) have band gaps that may be tuned across the near-infrared to visible parts of the spectrum (0.8–1.8 eV).² This makes them attractive candidates as light-harvesting elements in solar cells.^{3–5} Interest in these applications has surged in recent years, following the observation of multiple exciton generation (MEG) in PbS NCs, where the excess energy of an absorbed photon is used to generate extra electron–hole pairs, rather than being wasted to heat.^{6–8} The collection of multiple excitons in a PbS-sensitized TiO₂ photovoltaic device has been demonstrated.⁹

The majority of synthetic approaches to PbS and other lead chalcogenides have used colloidal routes, where capping by an organic ligand is used to achieve size selection and provide some surface passivation.^{2,10–12} However, in recent years, the stability of these NCs in air has been questioned, with the demonstration of very rapid oxidation of the outer surfaces of colloidal NCs of PbS⁶ and PbSe.¹³ In the case of PbS, up to

two-thirds of the volume of the NC may be oxidized after a few hours' exposure to air.⁶ Such oxidation is particularly undesirable as it reduces the diameter of the core of the NC, blue-shifting its optical absorption.^{6,13} There is therefore an urgent need to find a synthetic route to more stable PbS NCs; routes that allow for the direct synthesis of a conformal film are particularly attractive as these films may be directly usable as part of a functional device, reducing the number of processing steps.

These considerations have led us to investigate the synthesis of PbS NC films at the interface of two immiscible liquids (in this case toluene and water). This approach has recently been developed as a benign and generic soft-chemical medium for the deposition of nanocrystalline thin films of materials ranging from metals (Au, Ag),¹⁴ wide gap oxides (CeO₂),¹⁵ and chalcogenides including CdS^{14,16} and PbS.¹⁷ When appropriate precursors are dissolved in the aqueous and organic layers, the interface introduces steep gradients in ionic concentration with

Received: December 9, 2014

Published: January 4, 2015

critical lengths on the order of nanometres, because of the limited mixing of the liquids at the interface. These gradients can create a spatially confined region of supersaturation that allows the growth of films of low-dimensional crystallites. Fan et al. demonstrated that large (500 nm) crystallites with high energy {113} facets can be obtained through the liquid–liquid route;¹⁷ however, these crystals are too large to show quantum confinement. Here we extend this work, demonstrating the synthesis of NCs of 10–40 nm diameter using lead thiobiuret [$\text{Pb}(\text{SON}(\text{CN}^{\text{i}}\text{Pr}_2)_2)_2$, PTB] and lead diethyldithiocarbamate [$\text{Pb}(\text{S}_2\text{CNEt}_2)_2$, PDETC] precursors. The lead precursor in toluene is layered on top of an aqueous layer containing the sulfur precursor (Na_2S) in a beaker, and the films that form at the interface transferred to a substrate.

In the liquid–liquid synthesis route, size selection is achieved in the main by the pressure supplied by the volume of liquid overlying the interface,¹⁷ rather than by use of a capping ligand. It is then of some importance to examine the surface chemistry of the resulting NCs, and in particular their stability in air. This work requires us to characterize the depth-dependent composition of the NCs. Depth-profiling X-ray photoelectron spectroscopy (XPS) using synchrotron radiation (SR) as the exciting source is one of very few techniques that can provide this information, because the tunability of SR allows the photoelectron inelastic mean free path length, and hence the sampling depth to be varied over distances commensurate with the nanoparticle size.^{6,18–21} We have previously used this approach to characterize surface oxidation in colloidal PbS and PbS/PbSe NCs.^{6,2,10}

Here, we apply SR-excited depth-profiling to the surface oxidation of PbS NC films prepared via the liquid–liquid route, studying air-exposed films at intervals of up to 9 months after synthesis. Bulk mineral PbS (galena) is the most important lead mineral,²² and thus, its oxidation is an important reaction in mineral beneficiation using froth flotation, and in the extraction of lead from ore using hydrometallurgical operations such as leaching.^{23–25} A number of XPS investigations of the oxidation of natural single crystal PbS^{23,26–30} and the dissolution²⁵ and acid leaching of powdered PbS^{24,31} in aqueous solution have been carried out. Some conflicting conclusions have been reached about both the lead and sulfur species formed during the oxidation reaction.²³ While the final oxidation product includes SO_4^{2-} , the nature of the intermediate sulfur oxidation products has been extensively debated,²⁷ and the proposed lead-containing products include hydrated lead oxide,³⁰ hydroxide,^{30,26,31} carbonate,^{23,26} and thiosulfate.³¹ The question of whether or not the reaction proceeds congruently (with dissolution of Pb and S in equivalent amounts) remains open.^{28,30,32} The time- and depth-dependent study undertaken in this work allows us to demonstrate that the initial oxidation of PbS NC films is incongruent, with reaction of Pb to form $\text{Pb}(\text{OH})_2$ species before significant oxidation of sulfur. This results in the creation of a lead-deficient Pb_{1-x}S phase, which is detected in XPS. A surface-passivation layer of sulfite and sulfate is created after more extensive exposure to air. We compare our work with XPS studies of the oxidation of colloidal PbS NCs^{2,6,33–35} and show that the surfaces of NCs prepared through the liquid–liquid route can be more stable to aerial oxidation, an important criterion for their use in future solar devices.

2. EXPERIMENTAL SECTION

2a. Synthesis. *Synthesis of the Lead Thiobiuret Precursor [$\text{Pb}(\text{SON}(\text{CN}^{\text{i}}\text{Pr}_2)_2)_2$].* A solution of *N,N*-diisopropylcarbamoyl chloride (1.0 g, 6 mmol) and sodium thiocyanate (0.49 g, 6 mmol) in acetonitrile (25 mL) was heated to reflux with stirring for 1 h. During this time a precipitate of sodium chloride was formed, which was removed via filtration. Diisopropylamine (1.49 mL, 12 mmol) was then added to the cooled reaction mixture, followed by a further 30 min of stirring. This was followed by the addition of lead(II) acetate (1.0 g, 3 mmol) and stirring for a further 30 min. The resulting pale-brown precipitate was collected by Buchner filtration and recrystallized from tetrahydrofuran. Elemental analysis: Calcd (%): C, 43.1; H, 7.1; N, 10.8; S, 8.2 Pb, 26.6. Found (%): C, 43.0; H, 7.9; N, 10.7; S, 8.1; Pb, 26.5.

Synthesis of Lead Diethyldithiocarbamate [$\text{Pb}(\text{S}_2\text{CNEt}_2)_2$]. Sodium hydroxide (0.4 g, 10 mmol) was added to methanol (40 mL) to form a solution. Diethylamine (1.1 mL, 10 mmol) was added to this solution, followed by the dropwise addition of carbon disulfide (0.6 mL, 10 mmol). Immediately following the addition of the carbon disulfide, a solution of lead(II) acetate (1.0 g, 3 mmol) in methanol (40 mL) was added, and the resulting mixture stirred vigorously to avoid polymerization. The lead DETC was then formed as a pale-brown precipitate, and was collected via filtration and dried to form a pale yellow solid. Elemental analysis: Calcd (%): C, 23.8; N, 4.0; H, 5.6. Found (%): C, 24.5; N, 4.1; H, 5.6.

Deposition of Lead Sulfide Films. In a typical experiment, the lead-containing precursor was dissolved in toluene (30 mL, 1 or 2 mM) and layered upon an aqueous solution of sodium sulfide nonahydrate, $\text{Na}_2\text{S}\cdot 9\text{H}_2\text{O}$ (30 mL, 1 or 2 mM), in a 100 mL beaker with a diameter of 4.5 cm (corresponding in this case to a solvent height of 19 ± 1 mm; solvent heights of $(16\text{--}25) \pm 1$ mm were explored). In the case of the lead thiobiuret precursor, a portion of the toluene (10 mL) was replaced with 1-octanol to facilitate dissolution. After the layers had settled, the beaker was placed in an oven at a temperature of 50 °C for 2 h. During this time, a visible brown-gray film was formed at the interface. The solvent layers remained colorless throughout. The toluene layer was then removed by pipet, and the film deposited directly onto glass or ITO (tin-doped indium oxide)-coated glass substrates. The films were characterized as described below and then stored in air for periods of up to 9 months before introduction to vacuum for study by XPS.

2b. Characterization. X-ray diffraction (XRD) of samples deposited on glass slides was performed using a Bruker D8 Discover diffractometer using monochromated $\text{Cu K}\alpha$ radiation. Transmission electron microscope (TEM) imaging was performed using an FEI Tecnai TF30 microscope equipped with a field emission gun (FEG) and operated at 300 kV. Samples were deposited onto carbon-film-coated copper grids immediately following synthesis by transferral from the glass slides before solvent evaporation. XPS was performed using beamlines at two synchrotron sources, the BACH beamline ($35 < h\nu < 1600$ eV, equipped with a VSW 150 mm mean radius hemispherical electron energy analyzer) at the Elettra synchrotron in Trieste, Italy, and beamline I311 ($43 < h\nu < 1500$ eV, equipped with a Scienta SES200 hemispherical electron energy analyzer) at MAX-lab in Lund, Sweden. XPS spectra were recorded at room temperature at a total instrumental resolution of 170 meV (at 250 eV photon energy) to 1.26 eV (at 1400 eV photon energy), and in normal emission geometry. Binding energies were calibrated to C 1s at 284.8 eV BE (binding energy). Quantification of the XPS data is described in the Supporting Information.

3. RESULTS AND DISCUSSION

3a. Film Characterization. PbS NCs were obtained as pale gray deposits at the interface between the toluene solution containing the Pb precursor and the aqueous Na_2S solution. X-ray diffraction patterns obtained from these films are characteristic of cubic PbS crystallites having the rock salt structure, with a preferred (002) orientation (Figure SI.1, Supporting

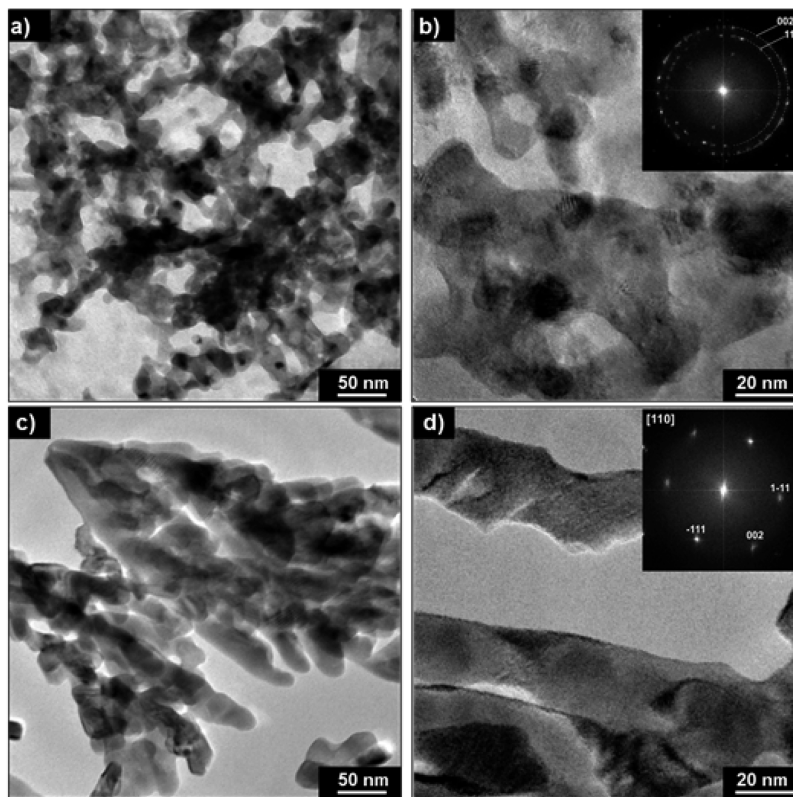


Figure 1. Low and high magnification TEM images for PbS thin films synthesized using PTB (a,b) and PDETC (c,d) precursor with 1:1 Pb/S molar ratio and a solvent height of 19 ± 1 mm. Insets show Fourier transforms of the images.

Information). Crystallite size estimates obtained from the Scherrer formula varied from 10 ± 3 to 40 ± 5 nm, depending on the choice of precursor and the lattice reflection (with the largest estimates obtained from the (002) reflection).

Experiments were performed using different Pb/S mole ratios and differing heights (and hence pressure) of the toluene solvent in the top layer, in order to determine the optimum conditions for NC synthesis. The nature of the final product was found to be relatively insensitive to the Pb/S mole ratio; NCs having the cubic PbS structure were formed for ratios varying between 1:2 and 2:1 Pb/S. In the case of the PDETC precursor, an increase in solvent pressure was found to reduce the size of the NCs produced (Figure SI.1, Supporting Information), reflecting rapid deposition under an increased degree of kinetic control,¹⁷ but no clear trend was obvious in the case of samples synthesized using PTB.

The morphology of the PbS NCs is very strongly influenced by the choice of precursor, as has been noted previously.¹⁷ Figures 1 and SI.2 (Supporting Information) show TEM analysis of films synthesized using PDETC and PTB precursors. TEM images of films synthesized using the PTB precursor typically show interconnected networks of 10–20 nm NCs (Figure 1a,b) in good agreement with corresponding crystallite size estimates obtained by applying the Scherrer equation to XRD data ($10\text{--}35 \pm 3$ nm). Selected area electron diffraction (SAED) data (Figure SI.2a) and Fourier transforms (FTs) of lattice resolution images (inset in Figure 1b) confirm that the NCs are cubic PbS (galena) and composed of randomly oriented nanosized crystals. In contrast, TEM imaging of films synthesized by the PDETC precursor are shown to consist of dendritic structures, each extending several 100 nm in size but with individual dendritic arms having widths of 20–50 nm

(Figure 1c,d). SAED patterns (Figure SI.2b) and FTs of HRTEM images (inset in Figure 1d) reveal these dendrites to be single crystals. The arms of the nanodendrites grow preferentially along the $\langle 111 \rangle$ directions, although the overall growth is not parallel to a single [111] type direction, leading to several individual dendrite arms having a zigzag morphology. Preferential growth along $\langle 111 \rangle$ directions is consistent with some previous reports of dendritic PbS growth.³⁶ The width of the individual dendritic arms perpendicular to the growth direction is much smaller than the size of the overall crystallite, consistent with complementary XRD data which yields an estimated minimum crystallite size of 38 ± 2 nm from the (002) reflection. Growth of such dendrites along all four $\langle 111 \rangle$ directions above a basal (001) plane leads to strong preferred (002) orientation in XRD,³⁶ as is observed here (Figure SI.1, Supporting Information).

3b. Surface Composition and Aging. In order to study the surface chemistry and composition of the NCs, synchrotron-excited depth-profiling XPS was carried out. For possible solar applications, a key parameter is the stability of the films in air. We have therefore studied the surface oxidation of air-exposed films having differing morphologies, prepared using both PTB and PDETC precursors at intervals of up to 9 months after synthesis. We begin by considering the XPS of freshly-synthesized samples, and the effect of particle size on the initial aerial oxidation.

Figure 2 shows the Pb 4f and S 2p core level XPS of a PbS film synthesized using PDETC precursor and a 1:1 Pb/S molar ratio (as in the TEM of Figure 1c,d). The samples were transferred into UHV for measurement within 1 week of synthesis, and the data are typical of those obtained from a large number of slightly aged films. Peak assignments are shown in

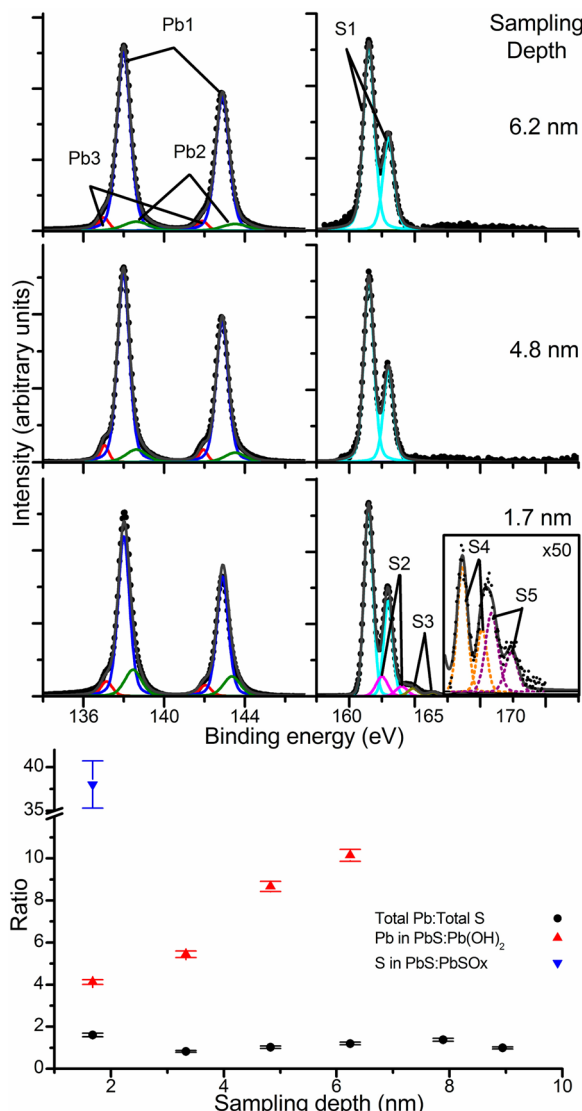


Figure 2. Pb 4f and S 2p XPS spectra recorded at different sampling depths for a PbS NC film synthesized using PDETC precursor with 1:1 Pb/S molar ratio and a solvent height of 19 ± 1 mm. Photon energies are 1000 eV (giving 6.2 nm sampling depth), 700 eV (4.8 nm), and 250 eV (1.7 nm). Sample has been exposed to air for approximately 1 week between synthesis and measurement. Quantification of the relative abundance of the Pb and S species from XPS is also shown as a function of sampling depth. Sulfur peaks due to PbSO_x (sulfite, S4 and sulfate, S5) could only be quantified at the lowest sampling depth used, and $\text{Pb}(\text{OH})_2$ (Pb2) could not be fitted for sampling depths above 6.2 nm. Estimated errors from XPS peak fitting are shown. Peak assignments are shown in Table 1.

Table 1. The predominant feature in the Pb 4f region is the strong doublet associated with PbS ($\text{Pb } 4f_{5/2}$ at 138 eV BE,⁶ Pb1, Table 1), but small tails to high and low BE, attributed respectively to oxidized lead (Pb2) and metallic lead (Pb3), are also observed.⁶ It is possible that the latter is created by degradation under the SR beam.⁶ It can be seen that the S 2p spectra show a strong signal in the 159–164 eV BE range, assigned to S^{2-} in PbS (S1), and much smaller components at higher BE labeled S2–S5. The latter are only visible at 250 eV photon energy. The S 2p core level shows large chemical shifts; any structure observed between ca. 165 eV BE and 171 eV BE may be attributed to strongly oxidized species (such as sulfate (S5, S^{6+}) and sulfite (S4, S^{4+})). From the low intensity of features in this BE range, it is apparent that very little surface oxidation has occurred during air storage. The S3 component has been attributed to surface S attached to two O atoms, $-\text{SO}_2$.^{27,37} Several assignments are possible for the S2 species. In studies of colloidal PbS NCs, it has been attributed to the surface S–C bond associated with the organic ligand.^{6,35} In our case, no passivating ligand is used, and the C 1s signal is of much lower intensity than is typical for colloidal NCs, but we cannot rule out the presence of small amounts of residual PDETC precursor. S2 has also been associated with sulfur atoms associated with one oxygen atom in surface $-\text{SO}$ moieties,²⁷ representing the very initial stages of oxidation. Its BE is also consistent with surface-adsorbed protons, in $-\text{SH}$ species.³⁸ We return to this point below.

The distribution of surface oxidation products was probed by varying the incident photon energy, and hence the photo-electron kinetic energy, which determines the photoelectron inelastic mean free path.^{6,19} The sampling depth from which 95% of the detected electrons originate is approximately 3 times the inelastic mean free path.⁴² Spectra were taken at sampling depths ranging between 1.7 and 8.4 nm⁴³ by varying the photon energy between 250 and 1400 eV (section S.4, Supporting Information). Examples are shown in Figure 2. It can be seen that as the sampling depth decreases, the intensity of the features due to oxidized lead (Pb2), neutral lead (Pb3), $-\text{SO}/\text{S–C}$ (S2), and $-\text{SO}_2$ (S3) increase. The intensity due to sulfate (S5) and sulfite (S4) is low throughout, but can be fitted at the lowest sampling depth used. These results indicate the presence of a very small amount of oxidation products, localized at the NC surfaces. This is in contrast to results obtained from colloidal PbS NCs which typically show a much larger degree of surface oxidation after a similar air exposure.⁶ The ratio of PbSO_x ($x = 3,4$)/PbS taken from the S 2p spectra at 1.7 nm sampling depth is approximately 0.03:1. This is around 30 times smaller than for similarly stored colloidal NCs,⁶ which typically show equivalent PbSO_x ($x = 3,4$)/PbS

Table 1. XPS Peak Assignments

peak label	assignment	literature binding energy (eV) ^a	observed binding energies (eV) ^a
Pb1	lead in PbS	138 ³⁹	138 ± 0.1
Pb2	lead in $\text{Pb}(\text{OH})_2/\text{Pb}_3(\text{OH})_2(\text{CO}_3)_2$	138.4 ^{40,41}	$138.4\text{--}138.6 \pm 0.1$
Pb3	neutral lead	136.8 ⁴¹	$137\text{--}137.1 \pm 0.1$
S1	sulfur in PbS	161.0 ³⁹	161.2 ± 0.1
S2	sulfur in $-\text{SO}/\text{S–C}/-\text{SH}$	162.3 ($-\text{SO}$) ²⁷ /162.0 (S–C) ³⁵ /162.2 ($-\text{SH}$) ³⁸	162.0 ± 0.2
S3	sulfur in $-\text{SO}_2$	163.9 ²⁷	163.9 ± 0.2
S4	sulfur in SO_3^{2-}	167.1 ²⁷	166.9 ± 0.2
S5	sulfur in SO_4^{2-}	168.8 ²⁷	168.7 ± 0.2

^aBEs are referenced to C 1s at 284.8 eV and refer to the low BE component of each multiplet.

ratios in the range 0.8:1–1.0:1. After correcting for variations in the relative photoionization cross sections with photon energy,⁴⁴ the total Pb/total S ratio obtained at every sampling depth studied, except the most surface sensitive (1.7 nm), is $1:1.0 \pm 0.2$, indicating that the NCs are approximately stoichiometric, except very close to the surface. The data suggest that lead enrichment is observed at the surface at this early stage of aging (Figure 2).

Next we explore the effect of a change in NC size (achieved by changing the pressure of the overlying solvent during synthesis). Figure 3 shows the Pb 4f and S 2p core level XPS of

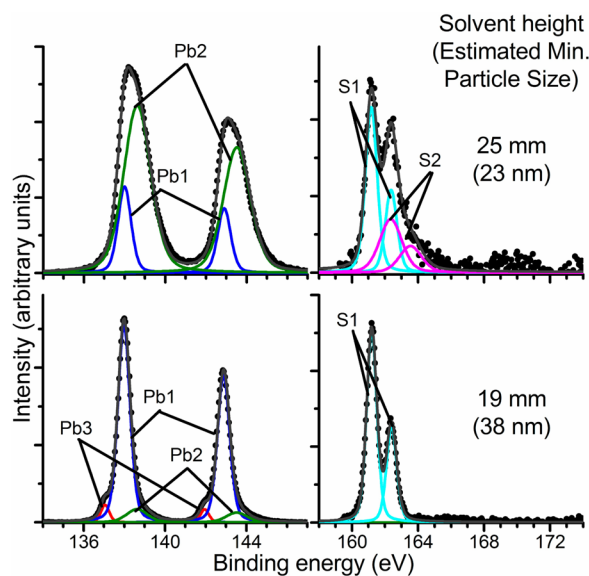


Figure 3. Pb 4f and S 2p XPS spectra recorded using 700 eV photon energy (sampling depth 4.8 nm) for PbS NC films synthesized using PDETC precursor with 1:1 Pb/S molar ratio and different solvent pressures, achieved by varying the solvent height above the synthesized film. Corresponding estimated minimum particle sizes from the (002) reflection in XRD are also indicated. Samples have been exposed to air for approximately 1 week.

PbS films synthesized using PDETC precursor, as a function of solvent pressure (given as solvent height above the synthesized film and corresponding to the XRD shown in Figure SI.1; estimated particle sizes are also shown). The samples have been exposed to air for approximately 1 week before data accumulation. The figure illustrates the marked changes that are observed in the XPS as the NC size decreases. For the smaller NCs, the XPS signals are broader, and (in particular) a very large Pb2 component, assigned to oxidized lead, is now visible. Indeed, this is the largest component observed in the Pb 4f spectrum (Figure 3). The Pb3 component due to neutral lead is no longer present. Although the S 2p spectrum is noisy, it can be seen that the S2 signal ($-SO/-SH/S-C$) is larger, and the sulfate (S5) and sulfite (S4) components (at BEs in the range 168–172 eV) are now more evident, although still of low intensity. The film having the smaller particle sizes has undergone more marked degradation in a fixed time, as we might expect if the initial rate of the degradation reaction depends on surface area. However, it is immediately obvious from the comparison between the Pb 4f and S 2p signals that the oxidized lead component (Pb2) is not accounted for by the amounts of $PbSO_3$, $PbSO_4$, or other sulfur-containing oxidation products. A large amount of oxidized lead has been formed without the formation of a correspondingly large amount of oxidized sulfur. This strongly suggests that the surface oxidation reaction is incongruent, with significant lead oxidation occurring before substantial oxidation of sulfur species. We investigate this hypothesis further by examining films aged for different times below.

Figure 4 shows the Pb 4f and S 2p core level XPS of PbS films (synthesized using PDETC precursor) for aging times of up to 9 months. (Additional data for films prepared using a range of Pb/S molar ratios are shown in the Supporting Information, Figures SI.3 and SI.4.) After aging in air for 1 week, the general features of XPS are similar to those seen in Figure 2, although with a larger oxidized lead (Pb2) component. This component does not show any strong variation in intensity with sampling depth. The corresponding S 2p spectra show vanishingly small features due to sulfate (S5)

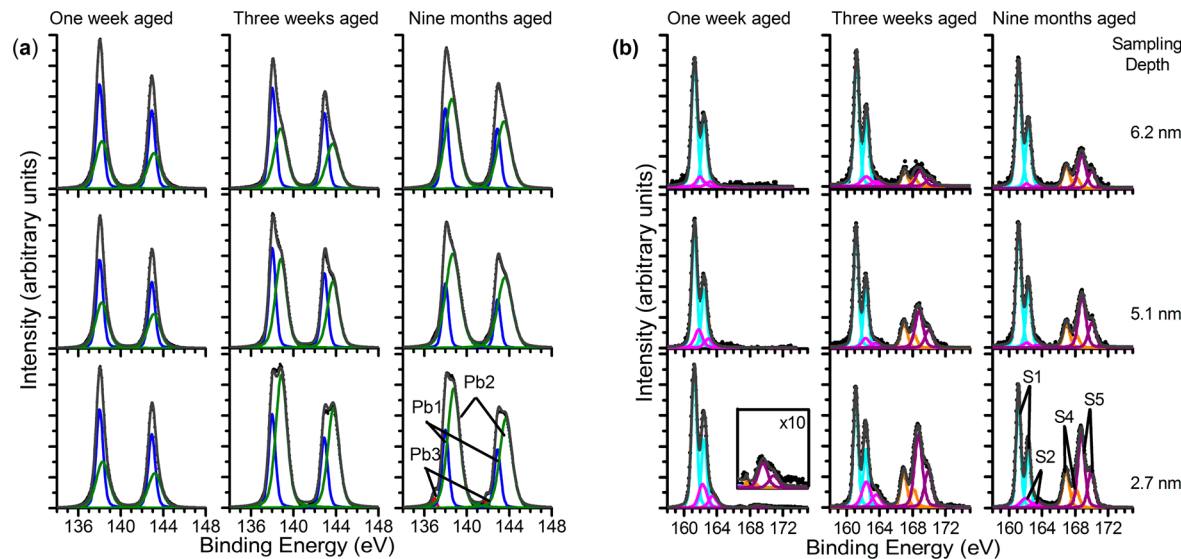


Figure 4. Effect of surface aging time in air on the Pb 4f (a) and S 2p (b) XPS spectra of a PbS NC film, recorded at different sampling depths. The film was synthesized using PDETC precursor with 1:2 Pb/S molar ratio and a solvent height of 19 ± 1 mm. Photon energies are 1000 eV (giving 6.2 nm sampling depth), 800 eV (5.1 nm), and 400 eV (2.7 nm).

and sulfite (S4), but there is a component due to $-SO/-SH/S-C$ (S2), which is largest at the lowest sampling depth used (3.3 nm). The picture at this early stage of aging is of a significant amount of oxidized Pb (possibly lead oxide, hydroxide, hydroxycarbonate, or hydrated oxide, discussed further below), which is *not* localized only at the topmost sample surface, together with a small amount of $-SO/-SH/S-C$ species that lie predominantly at the surface. Again, this suggests the oxidation reaction is incongruent, with substantial lead oxidation occurring before significant oxidation of sulfur. After aging in air for 3 weeks, and then for 9 months, the intensity of the oxidized lead (Pb2) component increases to become the dominant component of the Pb 4f multiplet. It now shows an increase in intensity at low sampling depth. The corresponding S 2p spectra show that strong signals due to sulfate (S5) and sulfite (S4) become visible after 3 weeks of aging. These signals increase in intensity as the sampling depth is decreased, and a similar variation is now observed in the Pb2 component. We note that $PbSO_3$ and $PbSO_4$, once formed, both contribute to the Pb 4f signal due to oxidized Pb (Pb2). Thus, after longer aging times (a few weeks), a surface layer of $PbSO_3$ and $PbSO_4$ is produced. The overall amount of strongly oxidized sulfur increases only slightly after further aging to 9 months, and this is accompanied by a *decrease* in the intensity of S2. This suggests that S2 here is predominantly associated with the initial stages of oxidation (i.e., $-SO$ or $-SH$ moieties^{27,38}) rather than the S-C bond of any residual precursor. Over prolonged aging periods, these species are oxidized further to $PbSO_3$ and $PbSO_4$ as discussed further below. The depth distribution of $PbSO_3$ and $PbSO_4$, and the ratio of $PbSO_3$ (S4) to $PbSO_4$ (S5) are not significantly changed by aging to 9 months (although the amount of oxidized Pb sampled at larger sampling depths increases somewhat). This suggests that the outer sulfate/sulfite layer has a passivating effect on the underlying PbS. Figure 5 shows elemental quantification as a function of depth for the PDETC-synthesized film studied in Figure 4. After 1 week of aging, the ratio of total Pb/total S is

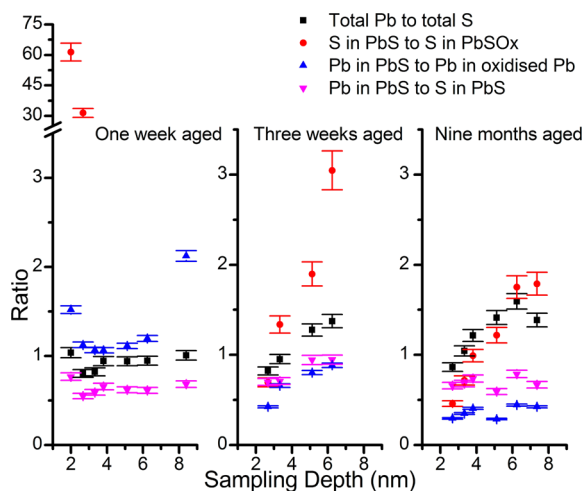


Figure 5. Quantification of the relative abundance of the Pb and S species during aging of a PbS NC film synthesized using PDETC precursor (as in Figure 4). Components S4 and S5 (i.e., sulfite and sulfate) are included in "S in $PbSO_x$ ", while the Pb2 component is here used to obtain the relative abundance of *all* oxidized species containing Pb ($Pb(OH)_2$ and Pb sulfite and sulfate formed after extended aging, see text). Estimated errors from XPS peak fitting are shown.

roughly 1:1, consistent with a starting composition of PbS, except at the lowest sampling depth used (1.7 nm), where the surface is again observed to be Pb-rich, as in Figure 2. However, during aging more marked variation with sampling depth becomes apparent, with the bulk becoming Pb-rich.

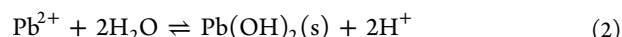
Broadly similar effects are observed in XPS when NCs synthesized using the PTB precursor are aged in air (Supporting Information, section S.3), although larger quantities of degradation products are produced after aging for 9 months (Figure SI.5). The PTB-synthesized samples typically consist of networks of roughly spherical 10–20 nm NCs, whereas the PDETC films are made up of larger and more crystalline particles with a smaller overall surface area. We would expect the former to oxidize faster; the rate of oxidation is discussed further below.

3c. Discussion. Our experiments allow us to make some comment about the nature of the initial Pb species formed during the early stages of oxidation, which has been a subject of some contention.^{23,26,30,31} It is clear from Figures 2 and 3 that this species cannot be attributed to lead thiosulfate, sulfite or sulfate, all of which have been proposed. Alternative assignments include PbO , $Pb(OH)_2$, $PbCO_3$, and the hydroxycarbonate $Pb_3(CO_3)_2(OH)_2$.^{30,31} The observed BE is most consistent with that of lead hydroxide,³⁰ and although PbO is more thermodynamically stable than the hydroxide, it is reasonable to expect surface hydroxide species in an ambient environment containing water vapor. In general, we do not observe strong carbonate features in C 1s XPS, although a detectable signal is present in cases where a large amount of the organic Pb precursor was used in synthesis. We assign the initial Pb2 component to $Pb(OH)_2$, although we cannot exclude the possibility of a small amount of the hydroxycarbonate. This is clearly formed before significant oxidation of S^{2-} to the S^{4+} state in species such as surface $-SO_2$ (S3) or sulfite (S4), or the S^{6+} state in sulfate (S5). However, we note that a small amount of $-SO/-SH$ (S2) is present at this stage of the degradation reaction.

The dissolution of PbS in aqueous solution^{25,31} and during anodic oxidation²³ has been extensively studied, although the mechanism remains unresolved. The initial step in aqueous solution has been proposed to be protonation of the lead sulfide surface,^{25,31} for example in



(Similarly, the formation of H_2S via interaction with two protons has also been proposed.²⁵) This reaction leads to rate-limiting²⁵ dissolution of equal amounts of lead and sulfur into solution, and ultimately to equivalent amounts of lead and sulfur oxidation products, that is, congruent dissolution. Fornasiero et al.³¹ have proposed that the lead ions are hydrolyzed to form $Pb(OH)_2$, which is ultimately readSORBED onto the PbS surface:

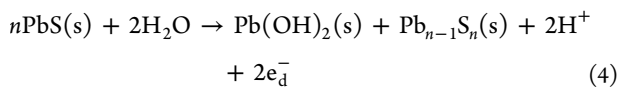


while at positive oxidation potentials or in the presence of oxygen, sulfate is ultimately formed through oxidation of the hydrogen sulfide ion, for example, in the anodic reaction:³¹

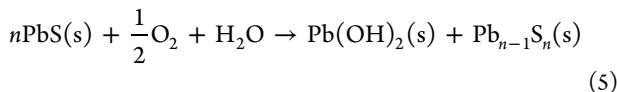


As the NC samples have been aged in air containing water vapor, we expect elements of the solution chemistry of PbS to be relevant. Feature S2 of the S 2p XPS may be associated with

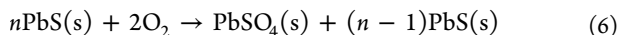
surface $-SH$ (or $-SO$) species, but it is nevertheless clear from Figures 3 and 4 that the surface oxidation of the NCs cannot be initiated *only* through a reaction of type (1). Even if the whole of the intensity of feature S2 is attributed to adsorbed $-SH$, a significant amount of the $Pb(OH)_2$ (component Pb2) remains unaccounted for and must be formed through a different route. By an extension of (2) to the solid surface, we propose that initial oxidation of the PbS occurs via



where e_d^- are defect electrons in $Pb_{n-1}S_n$. In the presence of O_2 , this may be accompanied by⁴⁵



These are incongruent reactions,⁴⁵ leading to a Pb -deficient PbS phase and a surface enriched in $Pb(OH)_2$ in the initial stages of reaction, as we observe (Figure 2). The ratio of Pb^{2+}/S^{2-} species found by XPS *within the PbS phase* is significantly less than 1 for aged samples (Figure 5), strongly supporting formation of Pb -deficient $Pb_{1-x}S$. We note that reaction 4 produces protons at the surface necessary to reaction 1, leading to the formation of surface $-SH$. This contributes to the S2 signal, which is the strongest signal observed due to S-containing reaction products in the early stages of degradation (Figures 2 and 4). The onset of reaction 1 then allows subsequent oxidation to proceed congruently with oxidation of the surface $-SH$, via $S(0)$, $-SO$, $-SO_2$ ²⁷ to sulfite and sulfate, giving reactions with overall stoichiometry of the type:



This may proceed in parallel with further incongruent reaction. The intensity of feature S2 associated with the $-SH/-SO$ intermediates clearly decreases in intensity as oxidation to sulfite/sulfate (S4/S5) proceeds (Figure 4). A feature due a neutral sulfur intermediate, $S(0)$, at an expected BE of around 163.5 eV²³ is not observed in these room temperature experiments. This is in accordance with substantial evidence showing that $S(0)$ formed on the PbS surface is very unstable in UHV and desorbs at room temperature; cryogenic temperatures are necessary for its observation.^{23,30,46} We note that while the initial Pb/S stoichiometry of the films is close to 1:1 (Figure 2), as the films age, they become increasingly Pb -rich in *overall* stoichiometry (i.e., when all Pb and S species are included) at all but the lowest sampling depths probed (Figure 5), supporting the idea that some S is lost from the surface during the later stages of oxidation.

As degradation proceeds, XPS shows that a surface layer of strongly oxidized sulfite and sulfate is formed (Figures 4, SI.3, and SI.4). As the flux of photoelectrons is attenuated according to the Beer-Lambert law as it emerges from the sample, it is possible to obtain an estimate of the thickness of the sulfite/sulfate layer at the NC surfaces by a simple model incorporating the inelastic mean free paths (described in section S4, Supporting Information^{19,47}). Figure 6 shows the resulting thicknesses in a typical case. The average thickness rises (roughly linearly with $\log(\text{time})$) to around 0.5 nm after 9 months. The logarithmic dependence shows that sulfite/sulfate formation slows with time, suggesting surface passivation by these species.³⁰ The behavior observed is similar to that

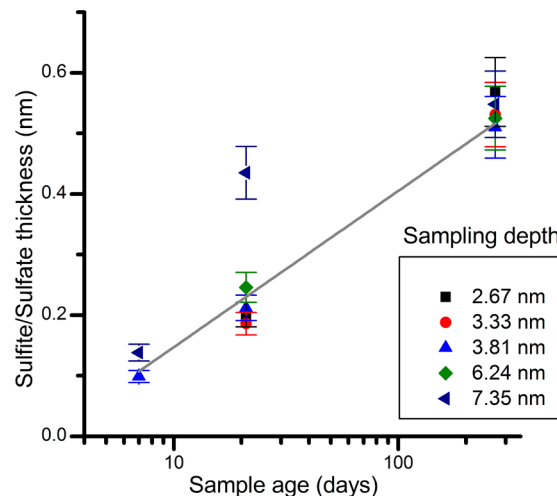


Figure 6. Sulfite/sulfate surface layer thicknesses (estimated from XPS using the approach of Shard⁴⁷) as a function of $\log(\text{surface aging time})$ for a PbS NC film. The film was synthesized using PDETc precursor and a 1:1 Pb/S molar ratio.

typically found in the surface passivation of metals^{48–50} (discussed further in section S5, Supporting Information). This typically shows a direct logarithmic growth law as we observe (Figure 6). We are unable to fit the data to the kinetic models developed for dissolution of PbS into solution,^{25,31} where the rate-limiting step is dissolution of the protonated surface by a reaction of the type shown in eq 1. This clearly indicates that when PbS is oxidized in air (rather than in solution) the sulfate/sulfite film that is formed at the surface by sulfur oxidation acts to passivate the surface to further attack, and the rate of reaction drops sharply as it becomes limited by ionic diffusion.

The layer thickness observed here after 9 months' exposure to air (around 0.5 nm) is the same as that found for colloidal 3.3 nm diameter nanoparticles⁶ after only a few hours' air exposure. Using the NC radii to estimate the surface area of a fixed volume, we find that the rate of sulfate/sulfite formation in the PDETc thin film (per unit surface area) is around 280 times slower than the colloidal NCs.⁵¹ This suggests that the surfaces of NCs prepared using PDETc through the liquid–liquid route are more stable to aerial oxidation than colloidal NCs. For PbS NCs produced without a covering of organic ligands, such as those synthesized here, we expect the lowest energy surfaces to be the {100} surfaces^{17,52} so we associate this stability with the highly crystalline nanodendrite morphology which has a strong preferred (200) orientation. In contrast, colloidal PbS nanocrystals are roughly spherical, showing as a minimum {200}, {220}, and {111} faces (the latter stabilized by ligand-induced surface reconstruction).⁵²

4. CONCLUSIONS

We have demonstrated the synthesis of 10–40 nm PbS NC films at the interface of toluene and water using lead thiobiuret and lead diethyldithiocarbamate precursors. We have applied SR-excited depth-profiling to the surface oxidation of the PbS NC films, studying air-exposed films at intervals of up to 9 months after synthesis. The time- and depth-dependent study undertaken in this work allows us to demonstrate that the initial oxidation of PbS NC films is incongruent, with reaction of Pb to form lead hydroxide species occurring before the production

of significant amounts of sulfur oxidation products. This is supported by the observation of lead-deficient $Pb_{1-x}S$ in the XPS of aged samples, and by the depth distribution of the $Pb(OH)_2$ in the early stages of oxidation. We propose that subsequent sulfur oxidation occurs through a congruent route involving surface-adsorbed $-SH$ species, via species such as $-SO$, and ultimately results in the formation of SO_3^{2-}/SO_4^{2-} . The latter forms a layer of typical average thickness around 0.5 nm after prolonged aging. The growth kinetics of the sulfate/sulfite film follow a logarithmic rate law typical of the formation of a surface passivation layer. For NC films prepared using PDETC, we show that the rate of aging per unit surface area is significantly slower than colloidal NCs. We associate this with their high crystallinity and preferred (200) orientation. This suggests that the surfaces of NCs prepared through the liquid–liquid route can offer enhanced stability to aerial oxidation, an important criterion for their use in future solar devices.

■ ASSOCIATED CONTENT

S Supporting Information

XRD, TEM, and SAED of PbS NCs, depth-profiling XPS of PbS NCs prepared using PTB, depth-profiling XPS as a function of aging time for films prepared using PDETC and various Pb/S molar ratios, notes on quantification of XPS and surface passivation kinetics. This material is available free of charge via the Internet at <http://pubs.acs.org>.

■ AUTHOR INFORMATION

Corresponding Author

*E-mail: wendy.flavell@manchester.ac.uk.

Present Addresses

[†]K.L.S.: School of Chemistry, The University of Nottingham, University Park, Nottingham NG7 2RD, United Kingdom.

[#]P.J.T.: School of Chemistry, Bangor University, Bangor, Gwynedd LL572UW, United Kingdom.

Notes

The authors declare no competing financial interest.

■ ACKNOWLEDGMENTS

We thank the Engineering and Physical Sciences Research Council (EPSRC), U.K. for funding under Grants EP/G035954/1, EP/J021172/1 and the NowNano Doctoral Training Centre (EP/G03737X/1). We also acknowledge Defense Threat Reduction Agency Grant HDTRA1-12-1-0013. The work at Elettra and MAX-lab was funded under The European Community's Seventh Framework Programme (FP7/2007-2013) under Grant Agreement No. 226716 and by EPSRC travel Grant EP/H0020446/1. We thank the CNR-IOM technician, F. Salvador.

■ REFERENCES

- (1) Banyai, L.; Hu, Y. Z.; Lindberg, M.; Koch, S. W. 3rd-Order Optical Nonlinearities in Semiconductor Microstructures. *Phys. Rev. B* **1988**, *38*, 8142–8153.
- (2) Akhtar, J.; Malik, M. A.; O'Brien, P.; Wijayantha, K. G. U.; Dharmadasa, R.; Hardman, S. J. O.; Graham, D. M.; Spencer, B. F.; Stubbs, S. K.; Flavell, W. R.; Binks, D. J.; Sirotti, F.; El Kazzi, M.; Silly, M. A Greener Route to Photoelectrochemically Active PbS Nanoparticles. *J. Mater. Chem.* **2010**, *20*, 2336–2344.
- (3) Zhao, N.; Osedach, T. P.; Chang, L. Y.; Geyer, S. M.; Wanger, D.; Binda, M. T.; Arango, A. C.; Bawendi, M. G.; Bulovic, V. Colloidal PbS Quantum Dot Solar Cells with High Fill Factor. *ACS Nano* **2010**, *4*, 3743–3752.
- (4) Pattantyus-Abraham, A. G.; Kramer, I. J.; Barkhouse, A. R.; Wang, X. H.; Konstantatos, G.; Debnath, R.; Levina, L.; Raabe, I.; Nazeeruddin, M. K.; Gratzel, M.; Sargent, E. H. Depleted-Heterojunction Colloidal Quantum Dot Solar Cells. *ACS Nano* **2010**, *4*, 3374–3380.
- (5) Nozik, A. J. Nanoscience and Nanostructures for Photovoltaics and Solar Fuels. *Nano Lett.* **2010**, *10*, 2735–2741.
- (6) Hardman, S. J. O.; Graham, D. M.; Stubbs, S. K.; Spencer, B. F.; Seddon, E. A.; Fung, H. T.; Gardonio, S.; Sirotti, F.; Silly, M. G.; Akhtar, J.; O'Brien, P.; Binks, D. J.; Flavell, W. R. Electronic and Surface Properties of PbS Nanoparticles Exhibiting Efficient Multiple Exciton Generation. *Phys. Chem. Chem. Phys.* **2011**, *13*, 20275–20283.
- (7) Ellingson, R. J.; Beard, M. C.; Johnson, J. C.; Yu, P. R.; Micic, O. I.; Nozik, A. J.; Shabaev, A.; Efros, A. L. Highly Efficient Multiple Exciton Generation in Colloidal PbSe and PbS Quantum dots. *Nano Lett.* **2005**, *5*, 865–871.
- (8) Nair, G.; Geyer, S. M.; Chang, L. Y.; Bawendi, M. G. Carrier Multiplication Yields in PbS and PbSe Nanocrystals Measured by Transient Photoluminescence. *Phys. Rev. B* **2008**, *78*, 125325.
- (9) Sambur, J. B.; Novet, T.; Parkinson, B. A. Multiple Exciton Collection in a Sensitized Photovoltaic System. *Science* **2010**, *330*, 63–66.
- (10) Akhtar, J.; Afzaal, M.; Banski, M.; Podhorodecki, A.; Syperek, M.; Misiewicz, J.; Bangert, U.; Hardman, S. J. O.; Graham, D. M.; Flavell, W. R.; Binks, D. J.; Gardonio, S.; O'Brien, P. Controlled Synthesis of Tuned Bandgap Nanodimensional Alloys of PbS_xSe_{1-x} . *J. Am. Chem. Soc.* **2011**, *133*, 5602–5609.
- (11) Nozik, A. J.; Beard, M. C.; Luther, J. M.; Law, M.; Ellingson, R. J.; Johnson, J. C. Semiconductor Quantum Dots and Quantum Dot Arrays and Applications of Multiple Exciton Generation to Third-Generation Photovoltaic Solar Cells. *Chem. Rev.* **2010**, *110*, 6873–6890.
- (12) Hillhouse, H. W.; Beard, M. C. Solar Cells from Colloidal Nanocrystals: Fundamentals, Materials, Devices, and Economics. *Curr. Opin. Colloid Interface Sci.* **2009**, *14*, 245–259.
- (13) Sykora, M.; Koposov, A. Y.; McGuire, J. A.; Schulze, R. K.; Tretiak, O.; Pietryga, J. M.; Klimov, V. I. Effect of Air Exposure on Surface Properties, Electronic Structure, and Carrier Relaxation in PbSe Nanocrystals. *ACS Nano* **2010**, *4*, 2021–2034.
- (14) Stansfield, G. L.; Vanitha, P. V.; Johnston, H. M.; Fan, D.; AlQahtani, H.; Hague, L.; Grell, M.; Thomas, P. J. Growth of Nanocrystals and Thin Films at the Water-Oil Interface. *Philos. Trans. R. Soc., A* **2010**, *368*, 4313–4330.
- (15) Mlondo, S. N.; Thomas, P. J.; O'Brien, P. Facile Deposition of Nanodimensional Ceria Particles and Their Assembly into Conformal Films at Liquid-Liquid Interface with a Phase Transfer Catalyst. *J. Am. Chem. Soc.* **2009**, *131*, 6072.
- (16) Mlondo, S. N.; Andrews, E. M.; Thomas, P. J.; O'Brien, P. Deposition of Hierarchical Cd(OH)₂ Anisotropic Nanostructures at the Water-Toluene Interface and Their Use As Sacrificial Templates for CdO or CdS Nanostructures. *Chem. Commun.* **2008**, *24*, 2768–2770.
- (17) Fan, D. B.; Thomas, P. J.; O'Brien, P. Pyramidal lead Sulfide Crystallites with High Energy {113} Facets. *J. Am. Chem. Soc.* **2008**, *130*, 10892.
- (18) Santra, P. K.; Viswanatha, R.; Daniels, S. M.; Pickett, N. L.; Smith, J. M.; O'Brien, P.; Sarma, D. D. Investigation of the Internal Heterostructure of Highly Luminescent Quantum Dot-Quantum Well Nanocrystals. *J. Am. Chem. Soc.* **2009**, *131*, 470–477.
- (19) Fairclough, S. M.; Tyrrell, E. J.; Graham, D. M.; Lunt, P. J. B.; Hardman, S. J. O.; Pietzsch, A.; Hennies, F.; Moghal, J.; Flavell, W. R.; Watt, A. A. R.; Smith, J. M. Growth and Characterization of Strained and Alloyed Type-II ZnTe/ZnSe Core-Shell Nanocrystals. *J. Phys. Chem. C* **2012**, *116*, 26898–26907.
- (20) Borchert, H.; Haubold, S.; Haase, M.; Weller, H. Investigation of ZnS Passivated InP Nanocrystals by XPS. *Nano Lett.* **2002**, *2*, 151–154.
- (21) Huang, K.; Demadrille, R.; Silly, M. G.; Sirotti, F.; Reiss, P.; Renault, O. Internal Structure of InP/ZnS Nanocrystals Unraveled by

- High-Resolution Soft X-ray Photoelectron Spectroscopy. *ACS Nano* **2010**, *4*, 4799–4805.
- (22) Vaughan, D. J. Sulfide Mineralogy and Geochemistry: Introduction and Overview. *Rev. Mineral. Geochem.* **2006**, *61*, 1–5.
- (23) Hampton, M. A.; Plackowski, C.; Nguyen, A. V. Physical and Chemical Analysis of Elemental Sulfur Formation during Galena Surface Oxidation. *Langmuir* **2011**, *27*, 4190–4201.
- (24) Abrafitis, P. K.; Patrick, R. A. D.; Kelsall, G. H.; Vaughan, D. J. Acid Leaching and Dissolution of Major Sulphide Ore Minerals: Processes and Galvanic Effects in Complex Systems. *Mineral. Mag.* **2004**, *68*, 343–351.
- (25) Hsieh, Y. H.; Huang, C. P. The Dissolution of PbS(S) in Dilute Aqueous-Solutions. *J. Colloid Interface Sci.* **1989**, *131*, 537–549.
- (26) Nowak, P.; Laajalehto, K. Oxidation of Galena Surface - An XPS Study of the Formation of Sulfoxyl Species. *Appl. Surf. Sci.* **2000**, *157*, 101–111.
- (27) Yashina, L. V.; Zyubin, A. S.; Puttner, R.; Zyubina, T. S.; Neudachina, V. S.; Stojanov, P.; Riley, J.; Dedyulin, S. N.; Brzhezinskaya, M. M.; Shtanov, V. I. The Oxidation of the PbS(001) Surface with O₂ and Air Studied with Photoelectron Spectroscopy and ab Initio Modeling. *Surf. Sci.* **2011**, *605*, 473–482.
- (28) Laajalehto, K.; Kartio, I.; Suoninen, E. XPS and SR-XPS Techniques Applied to Sulphide Mineral Surfaces. *Int. J. Miner. Process.* **1997**, *51*, 163–170.
- (29) Prince, K. C.; Heun, S.; Gregoratti, L.; Barinov, A.; Kiskinova, M. Long-Term Oxidation Behaviour of Lead Sulfide Surfaces. *Lect. Notes Phys.* **2002**, *588*, 111–120.
- (30) Buckley, A. N.; Woods, R. An X-Ray Photoelectron Spectroscopic Study of the Oxidation of Galena. *Appl. Surf. Sci.* **1984**, *17*, 401–414.
- (31) Fornasiero, D.; Li, F. S.; Ralston, J.; Smart, R. S. C. Oxidation of Galena Surfaces. 1. X-Ray Photoelectron Spectroscopic and Dissolution Kinetics Studies. *J. Colloid Interface Sci.* **1994**, *164*, 333–344.
- (32) Kartio, I.; Wittstock, G.; Laajalehto, K.; Hirsch, D.; Simola, J.; Laiho, T.; Szargan, R.; Suoninen, E. Detection of Elemental Sulphur on Galena Oxidized in Acidic Solution. *Int. J. Miner. Process.* **1997**, *51*, 293–301.
- (33) Asunsakis, D. J.; Bolotin, I. L.; Haley, J. E.; Urbas, A.; Hanley, L. Effects of Surface Chemistry on Nonlinear Absorption of PbS Nanocrystals. *J. Phys. Chem. C* **2009**, *113*, 19824–19829.
- (34) Lobo, A.; Müller, T.; Nagel, M.; Borchert, H.; Hickey, S. G.; Weller, H. Photoelectron Spectroscopic Investigations of Chemical Bonding in Organically Stabilized PbS Nanocrystals. *J. Phys. Chem. B* **2005**, *109*, 17422–17428.
- (35) Tang, J.; Brzozowski, L.; Barkhouse, D. A. R.; Wang, X. H.; Debnath, R.; Wolowiec, R.; Palmiano, E.; Levina, L.; Pattantyus-Abraham, A. G.; Jamakosmanovic, D.; Sargent, E. H. Quantum Dot Photovoltaics in the Extreme Quantum Confinement Regime: The Surface-Chemical Origins of Exceptional Air- and Light-Stability. *ACS Nano* **2010**, *4*, 869–878.
- (36) Ma, Y.; Qi, L.; Ma, J.; Cheng, H. Hierarchical, Star-Shaped PbS Crystals Formed by a Simple Solution Route. *Cryst. Growth Des.* **2004**, *4*, 351–354.
- (37) This species has also been attributed to thiosulfate, S₂O₃²⁻ (ref 31). As the two S atoms in thiosulfate have formal oxidation states of sulfate (+6) and sulfide (-2), this should give rise to two equally intense doublets, which are found between the BEs of PbS and PbSO₄ (ref 31). This is not observed here.
- (38) Leavitt, A. J.; Beebe, T. P. Chemical-Reactivity Studies of Hydrogen-Sulfide on Au(111). *Surf. Sci.* **1994**, *314*, 23–33.
- (39) Laajalehto, K.; Kartio, I.; Nowak, P. XPS Study of Clean Metal Sulfide Surfaces. *Appl. Surf. Sci.* **1994**, *81*, 11–15.
- (40) Nefedov, V. I.; Salyn, Y. V.; Solozhenkin, P. M.; Pulatov, G. Y. X-ray Photoelectron Study of Surface Compounds Formed during Flotation of Minerals. *Surf. Interface Anal.* **1980**, *2*, 170–172.
- (41) Pederson, L. R. Two-Dimensional Chemical-State Plot for Lead Using XPS. *J. Electron Spectrosc.* **1982**, *28*, 203–209.
- (42) Vickerman, J. C. *Surface Analysis - The Principal Techniques*; John Wiley and Sons: Chichester, 1997.
- (43) Tanuma, S.; Powell, C. J.; Penn, D. R. Calculations of Electron Inelastic Mean Free Paths. 3. Data for 15 Inorganic-Compounds over the 50–2000-eV Range. *Surf. Interface Anal.* **1991**, *17*, 927–939.
- (44) Yeh, J. J.; Lindau, I. Atomic Subshell Photoionization Cross-Sections and Asymmetry Parameters - 1 Less-Than-or-Equal-to Z Less-Than-or-Equal-to 103. *At. Data Nucl. Data* **1985**, *32*, 1–155.
- (45) Kim, B. S.; Hayes, R. A.; Prestidge, C. A.; Ralston, J.; Smart, R. S. C. Scanning-Tunneling-Microscopy Studies of Galena—The Mechanisms of Oxidation in Aqueous-Solution. *Langmuir* **1995**, *11*, 2554–2562.
- (46) Wittstock, G.; Kartio, I.; Hirsch, D.; Kunze, S.; Szargan, R. Oxidation of Galena in Acetate Buffer Investigated by Atomic Force Microscopy and Photoelectron Spectroscopy. *Langmuir* **1996**, *12*, 5709–5721.
- (47) Shard, A. G. A Straightforward Method For Interpreting XPS Data From Core–Shell Nanoparticles. *J. Phys. Chem. C* **2012**, *116*, 16806–16813.
- (48) Fehlner, F. P. Oxidation at Low-Temperatures. *Philos. Mag. B* **1985**, *52*, 729–738.
- (49) Xu, Z. J.; Rosso, K. M.; Bruemmer, S. Metal Oxidation Kinetics and the Transition from Thin to Thick Films. *Phys. Chem. Chem. Phys.* **2012**, *14*, 14534–14539.
- (50) Cabrera, N.; Mott, N. F. Theory of the Oxidation of Metals. *Rep. Prog. Phys.* **1948**, *12*, 163–184.
- (51) Estimate obtained using the average particle size of 38 nm from XRD.
- (52) Wang, Z. W.; Schliehe, C.; Wang, T.; Nagaoka, Y.; Cao, Y. C.; Bassett, W. A.; Wu, H. M.; Fan, H. Y.; Weller, H. Deviatoric Stress Driven Formation of Large Single-Crystal PbS Nanosheet from Nanoparticles and in Situ Monitoring of Oriented Attachment. *J. Am. Chem. Soc.* **2011**, *133*, 14484–14487.